Paramagnetic Palladacycles with Pd[III] Centers Are Highly Active Catalysts for Asymmetric Aza-Claisen Rearrangements

Simon H. Eitel,[†] Matthias Bauer,*,[‡] David Schweinfurth,[§,⊥] Naina Deibel,[§] Biprajit Sarkar,*,[§,⊥] Harald Kelm,[‖] Hans-Jörg Krüger,*,[‖] Wolfgang Frey,[†] and René Peters*,[†]

[†]Institut für Organische Chemie, Universität Stuttgart, Pfaffenwaldring 55, 70569 Stuttgart, Germany

[‡]Fachbereich Chemie, Technische Universität Kaiserslautern, Erwin-Schrödinger Straße Gebäude 54/684, 67663 Kaiserslautern, Germany

[§]Institut für Anorganische Chemie, Universität Stuttgart, Pfaffenwaldring 55, 70569 Stuttgart, Germany

[‖]Fachbereich Chemie, Technische Universität Kaiserslautern, Erwin-Schrödinger Straße Gebäude 54/655, 67663 Kaiserslautern, Germany

S *Supporting Information*
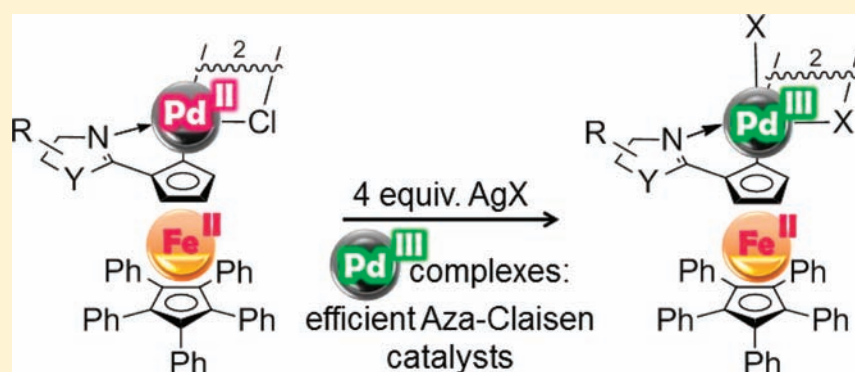
ABSTRACT: A combination of spectroscopic and electrochemical methods—XANES, EXAFS, X-ray, ^{1}H NMR, EPR, Mössbauer, and cyclic voltammetry—demonstrate that the most efficient Pd catalysts for the asymmetric rearrangement of allylic trifluoroacetimidates unexpectedly possess in the activated oxidized form a Pd[III] center bound to a ferrocene core which remains unchanged (Fe[II]) during the oxidative activation. These are the first recognized Pd[III] complexes acting as enantioselective catalysts.

1. INTRODUCTION

Recent studies of the fundamental chemistry of organometallic Pd[III] complexes have generated new impetus for the development of a better understanding of high oxidation state Pd species as key catalytic intermediates in carbon-heteroatom and carbon—carbon bond formations. These investigations implicate bimetallic Pd[III] catalysis as a mechanistic alternative to Pd[II]/Pd[IV] redox cycles.[1] A small number of organometallic dimeric Pd[III] complexes have been reported, in which a Pd—Pd single bond causes a diamagnetic behavior.[2] Isolated paramagnetic mononuclear organometallic Pd[III] complexes are even more rare and demonstrate a distinct reactivity profile.[3,4] Monomeric organometallic Pd[III] species were also proposed to be formed from Pd[II] complexes in the presence of ferrocenium or Ag[I] additives as catalytically relevant intermediates.[5a,6] In the latter case Ag[I] is assumed to initially bind to a Lewis basic Pd[II] center triggering an inner sphere electron transfer to form Pd[III] and Ag[0].[5] To our knowledge dimeric paramagnetic organometallic Pd[III]/Pd[III] complexes have not been described.[7]
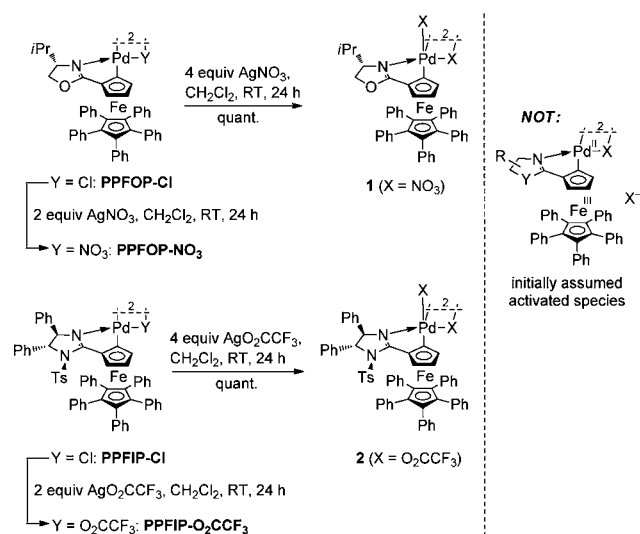
Herein we report spectroscopic evidence for dimeric paramagnetic ferrocene-derived palladacycles containing two Pd[III] centers, which are not involved in a Pd—Pd bond. These scalemic complexes were recently demonstrated to be the most efficient enantioselective catalysts for the rearrangement of allylic trifluoroacetimidates in terms of catalyst turnover numbers, scope and enantioselectivity and were initially suggested to be ferrocenium palladacycles containing a traditional Pd[II] center as catalytically active site (Scheme 1, right).[8,9]

2. RESULTS AND DISCUSSION

2.1. Catalyst Activation. Activation of the diamagnetic dimeric chloride-bridged pentaphenylferrocene oxazoline and imidazoline palladacycle precatalysts **PPFOP-Cl** and **PPFIP-Cl** occurred in quantitative yield by treatment with AgNO$_3$ and AgO$_2$CCF$_3$ (4 equiv, Scheme 1, left), respectively, and can be

Scheme 1. Catalyst Activation of the Dimeric Precatalysts by Treatment with Ag^I Salts

Scheme 2. Effect of Catalyst Oxidation by a Silver Salt on the Formation of Rearrangement Product 4a^a

^{a}The chloride counterions are exchanged with $y = 2$ equiv of silver salt per precatalyst dimer. With $y = 4$ the complexes are also oxidized.

described as a two-step process. Two equivalents of the corresponding silver salt are required for a Cl$^-$ counterion exchange (formation of **PPFOP-NO$_3$** or **PPFIP-O$_2$CCF$_3$** in Scheme 1) while another 2 equiv oxidize the complexes to provide the dark red-brown paramagnetic species **1** and **2** which show very broad signals in ^{1}H NMR.

A mixture of Ag and AgCl thus precipitates as a gray solid during the activation and has been separated by centrifugation for analysis. By microanalysis the Cl content was determined to be 18.91 wt % (expected for pure AgCl: 24.74 wt %, for a mixture of AgCl/Ag (1:1): 14.11 wt %). This corresponds to a ratio AgCl/Ag (1:0.41). These data were confirmed by EDX measurements (Ag content: 81.33 wt %, Cl content: 18.67 wt %).

The oxidation is indispensable for high activity in allylic imidate rearrangements using palladacycles derived from 2-ferrocenyl oxazolines[10,8d] or imidazolines.[8] For instance, rearrangement of model substrate **3a** gave only trace amounts of allylic amide **4a** with ferrocene imidazoline palladacycle precatalyst **FIP-Cl** (5 mol %) activated with 2 equiv of AgO$_2$CCF$_3$ per precatalyst dimer (Scheme 2), whereas activation with 4 equiv of the same silver salt gave the product in 88% yield under otherwise identical reaction conditions.[8a,d] Similarly, 0.2 mol % of **PPFOP-Cl**, activated by 2 equiv of AgNO$_3$, furnished **4a** in a yield of 45% after 24 h at 40 °C, whereas the same precatalyst provided a quantitative yield of **4a** after activation with 4 equiv of the same silver salt, although the catalyst loading was decreased by a factor of 4 (0.05 mol %) in the latter case.[8a,d]

We have previously interpreted this effect by the assumption that an Fe^{III} center in a ferrocenium core would decrease the electron density of the active Pd^{II} center by electronic communication thus generating a more Lewis acidic Pd^{II} center.[8d] Herein we provide spectroscopic evidence that this electronic communication in the activated species is better described by a resonance structure in which the actual spin density is basically localized at the Pd center directly after the activation by silver ions. That means an Fe^{II}/Pd^{III} complex is the activated catalyst species, in which Pd^{III} acts as a Lewis acid with largely enhanced activity as compared to the Pd^{II} complexes.
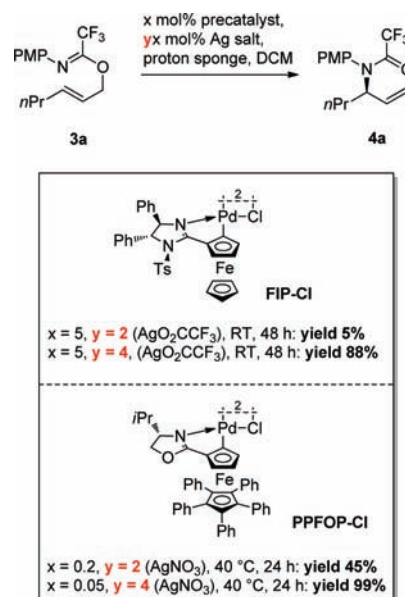
2.2. Spectroscopic and Electrochemical Studies. *X-ray Absorption Spectroscopy.*

The activation process was investigated by X-ray absorption near edge spectroscopy (XANES).[11] In Figure 1, the iron K-edge (7.112 keV) spectra of both catalytic systems are shown. Although in general the position and intensity of a prepeak at around 7118 eV are characteristic of the Fe oxidation state,[12] its intensity is usually low since the underlying 1s → 3d transition is dipole forbidden and of low intensity.[13] In case of ferrocene compounds the edge region itself, containing a characteristic 1s → Cp(π^*) transition at around 7121 eV is a better suited probe.[11] The Fe K-edge spectra were compared to those of pentaphenylferrocene and pentaphenylferrocenium tetrafluoroborate (Figure 1). Obviously, the ferrocene moiety of the palladacycles is not affected, neither by a Cl$^-$ to X$^-$ ligand exchange, nor by oxidation with a Ag^I salt. The intensity of the 1s → Cp(π^*) transition remains the same in all samples of the palladacycles, and the sharp feature of the ferrocenium complex is not observed.[11] Accordingly, iron remains in the oxidation state of Fe^{II} during the oxidation step of the catalyst activation.

In addition, palladium XANES data were recorded at the Pd L3-edge (3.173 keV, Figure 2). Since the 2p3/2 → 4d transition is dipole allowed, the edge transitions contain high intensity spectral information about the d-states, which are directly involved in redox processes. Investigations of the Pd L3-edge are still very rare[14] and have not been reported before for organometallic compounds. The spectra of the **PPFOP** and **PPFIP** systems are shown in Figure 2 (top and middle), together with their first derivatives allowing for a more precise localization of the white line position, i.e. the first resonance after the edge jump, which was used in previous studies of inorganic Pd complexes as indicator of the oxidation state.[14] Figure 2 reveals that the position of the white line changes continuously with the addition of 2 and 4 equiv of the corresponding Ag salt by 0.2 or 0.3 eV, respectively. The first shift after addition of 2 equiv of a Ag salt is caused by ligand
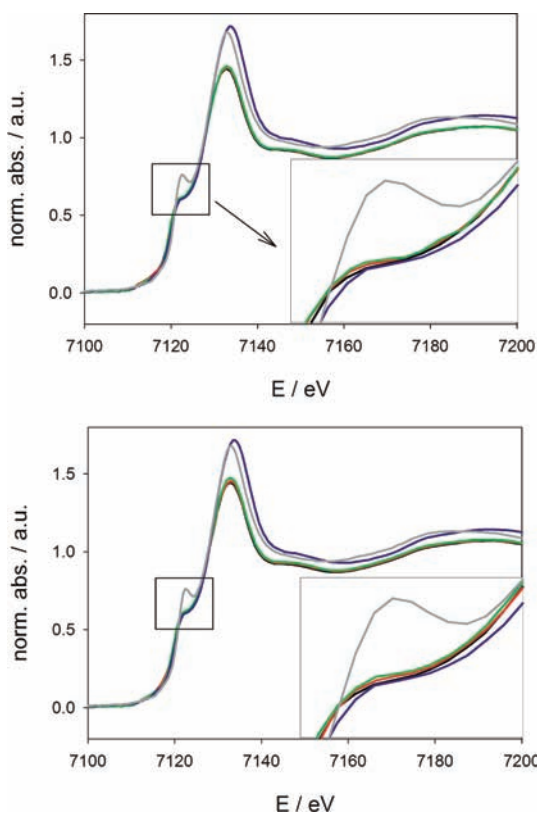
Figure 1. Fe K-edge XANES spectra of **PPFOP** (top) and **PPFIP** (bottom) systems. **PPFOP-Cl** and **PPFIP-Cl** (black), **PPFOP-ONO₂** and **PPFIP-O₂CCF₃** (red), and **1** and **2** (green) are compared to the references pentaphenylferrocene (blue) and pentaphenylferrocenium tetrafluoroborate (gray). The area of the $1s \rightarrow Cp(\pi^*)$ transition is enlarged in the insets.

effects at Pd^{II}, whereas the second one is a consequence of a reduced electron density at the Pd center.

For comparison of the oxidation state effect at the Pd L3-edge, the known $[Pd^{x+}([9]aneN_3)_2](Cl)_x$ complexes with $x = 2$, 3, and 4 were prepared according to the procedure by McAuley (Scheme 3).[4e] This systematic complex row was studied as reference system, in which only the oxidation state of Pd changes from +2 to +3 to +4, but not the coordinating atoms.

The corresponding L_3-edge spectra are shown in Figure 3. Only slight shifts of 0.2 eV in energy can be observed for this systematic row confirming the previous conclusions. It should be noted here that the area under the absorptions spectra did not show a trend in following the palladium oxidation states.

To get information about the geometric structure of the activated catalyst, Pd K-edge XAS measurements were carried out. The instructive Fourier transformed EXAFS spectra of **PPFIP-Cl** and **2** are shown in Figure 2 (bottom). The results obtained by fitting the experimental spectra with theoretical models are given in Table 1. In the fitting procedure of **PPFIP-Cl**, the coordination numbers were fixed to crystallographic values,[8] i.e., a combined C/N shell (from the imidazoline and Cp ligands) and two chlorides and, in addition, one Pd backscatterer since a dimeric structure is present. A carbon shell representing remote carbon atoms from the Cp and imidazoline is also included, but its coordination number is not reliable as is well-known.[15] The obtained distances agree quite well with the XRD values (see below).
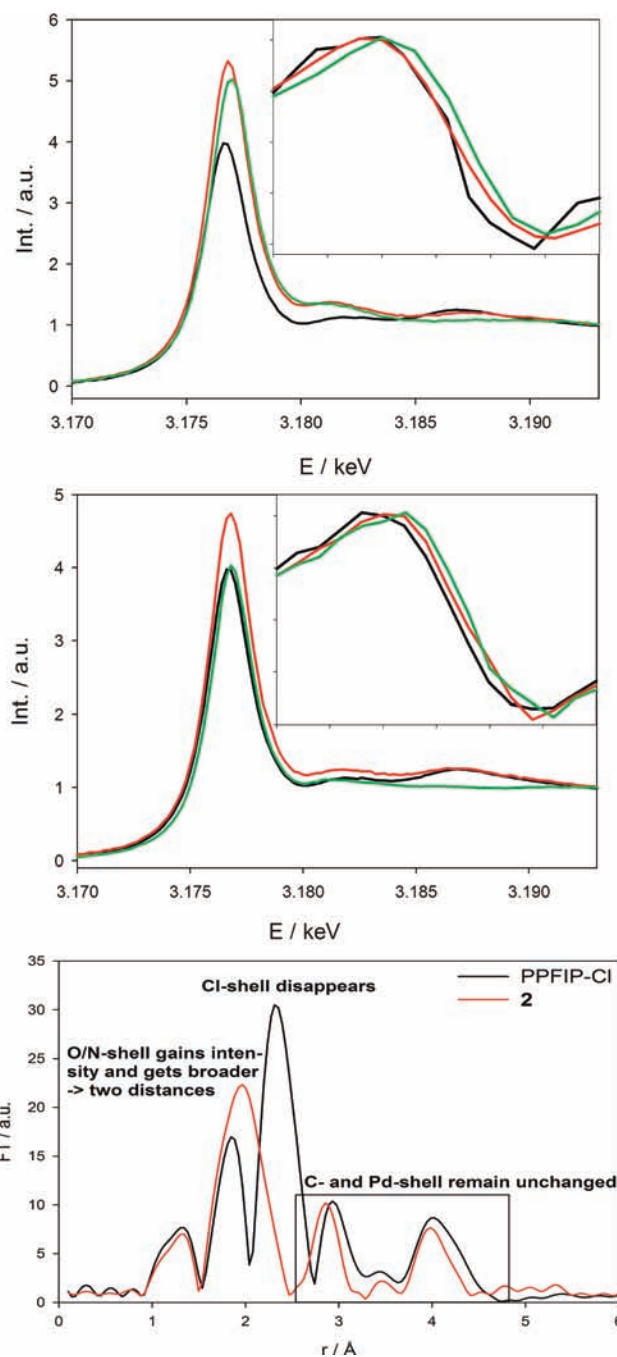

Figure 2. Top: Pd L_3-edge XANES spectra: **PPFOP-Cl** (black line), **PPFOP-ONO₂** (red line), and **1** (green line) are compared. The first derivatives of the edge region are shown as inset. Middle: Pd L_3-edge XANES spectra: **PPFIP-Cl** (black line), **PPFIP-O₂CCF₃** (red line), and **2** (green line) are compared. The first derivatives of the edge region are shown as inset. Bottom: Fourier transformed EXAFS functions obtained at the Pd K-edge for **PPFIP-Cl** and **2**.

After the activation, no chloride shell could be detected anymore, but still a Pd–Pd contact is visible, i.e., the dimeric structure remains intact. This is further supported by the identical Debye–Waller factor before and after activation and the identical Pd–Pd distances within the error bar. A metallophilic Pd–Ag contribution in the oxidized species can be excluded, since the heavy atom (Pd–Pd) coordination number remains the same, and no additional shell could be fitted. This is confirmed by inductively coupled plasma optical
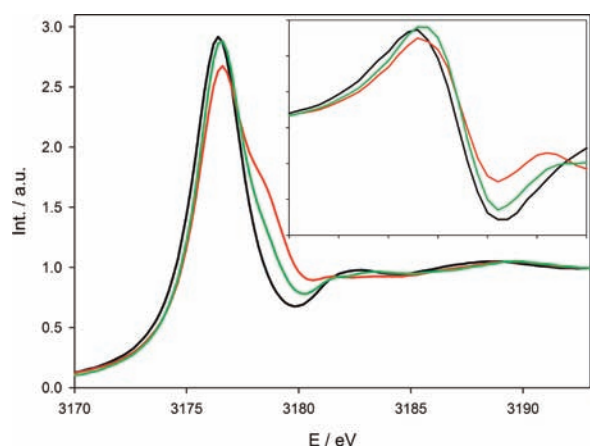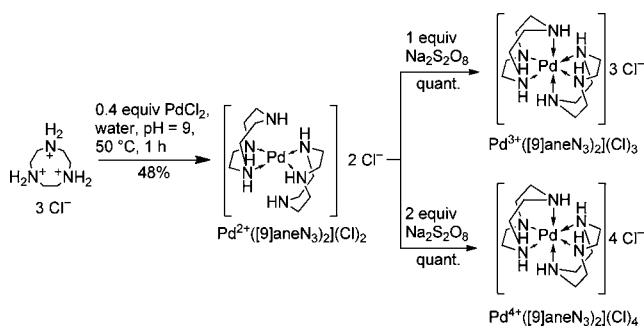
Scheme 3. Preparation of Pd^{x+}([9]aneN$_3$)$_2$](Cl)$_x$ Complexes with x = 2, 3, and 4[4e]

Figure 3. Pd L$_3$-edge XANES spectra of the [Pd^{x+}([9]aneN$_3$)$_2$](Cl)$_x$ reference system: x = 2 (black line), 3 (red line), and 4 (green line) are compared. The first derivatives of the edge region are shown as inset.

emission spectroscopy (ICP-OES) which detected no or just traces of Ag in the activated catalysts **1** and **2**, respectively (see the Supporting Information). The remaining fitted C/N/O shell, as composed of the imidazoline, Cp and trifluoroacetate ligand, contains 4.7 ± 0.5 backscatterers, in acordance with a 5-fold coordination geometry at the palladium center. The rather high Debye−Waller factor reflects the combination of three ligands in one shell. No significant changes can be detected in the higher distanced Pd−C shell, which is a further indicator for the intact structure of the complex.

The EXAFS results are in agreement with ESI-MS data for **1** and **2**, which reveal a dimeric aggregation of the activated catalysts **1** and **2** by detection of [**1** − NO$_3$]$^+$ and [**2** − O$_2$CCF$_3$]$^+$. Additional support of the drawn conclusions from the preceding X-ray absorption studies is supplied by the K-

edge XANES spectra of **PPFIP-Cl** and **2** presented in Figure 4. Although a shift in K-edge spectra can, in principle, also be
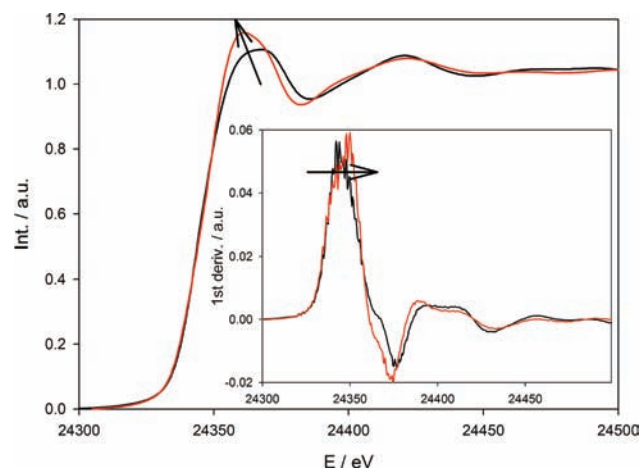

Figure 4. Pd K-edge XANES spectra of **PPFIP-Cl** (black line) and complex **2** (red line). The first derivatives of the edge region are shown as inset, the shift in the edge position and the increase in the white line intensity in complex **2** are highlighted by arrows.

caused by changes in the ligand sphere, it is attributed in case of **2** to an increase in the oxidation state to Pd^{III} compared to **PPFIP-Cl**. This oxidation state change follows from the increase of the white line intensity, which is characteristic for increased oxidation states in molecular complexes.[16]

EPR Studies. The X-ray absorption studies are supported by EPR measurements. The ferrocenium ion with a ^{2}E$_{2g}$ [(a$_{1g}$)^2(e$_{2g}$)^3] ground state is a typical organometallic example for a system with an exceptionally fast spin−lattice relaxation phenomenon, because the high symmetry of the ferrocenium ion leads to unequally filled degenerate orbitals.[17] Consequences of this are the observation of EPR signals only at very low temperatures (<20 K) due to high line broadening and a large g-anisotropy with one g value greater than 4 and the other close to 1.3. Substitution of alkyl or aryl groups in the Cp rings does not change the situation much.[17a] For the present case, a standard for the Fe^{III} center was set by 1,2,3,4,5-pentaphenylferrocenium hexafluorophosphate. As expected due to the fast spin−lattice relaxation this species does not show any EPR signal down to liquid nitrogen temperatures. Similarly, the oxidized forms of the pentaphenyl ferrocene imidazoline and oxazoline ligands are EPR silent down to liquid nitrogen temperatures. In contrast, **2** (either generated electrochemically from **PPFIP-Cl** or chemically as shown in Scheme 1) showed an EPR signal at 110 K both in the solid state (Figure 5, top)

Table 1. Results of the Analysis of the Pd K-Edge Spectra Obtained for PPFIP-Cl and Complex 2

sample	Abs−Bs[a]	N(Bs)[b]	R(Bs)[c]/Å	σ[d]/Å^2	FI (10^{-2})[e]
PPFIP-Cl	Pd−N/C	2*[f]	1.97 ± 0.02	0.011 ± 0.001	0.125
	Pd−Cl	2*	2.35 ± 0.02	0.013 ± 0.001	
	Pd−C	1.1 ± 0.3	2.87 ± 0.03	0.002 ± 0.001	
	Pd−Pd	1*	3.78 ± 0.04	0.017 ± 0.004	
2	Pd−C/N/O	4.7 ± 0.5	2.05 ± 0.02	0.021 ± 0.002	0.061
	Pd−C	1.6 ± 0.5	2.89 ± 0.03	0.002 ± 0.001	
	Pd−Pd	0.8 ± 0.2	3.81 ± 0.04	0.018 ± 0.004	

[a]Abs = X-ray absorbing atom, Bs = backscattering atom. [b]Number of backscatterers. [c]Distance between absorber and backscatterer. [d]Debye−Waller like factor. [e]Quality of fit. [f]Coordination numbers marked by an asterisk were set to the crystallographic values during the fit.
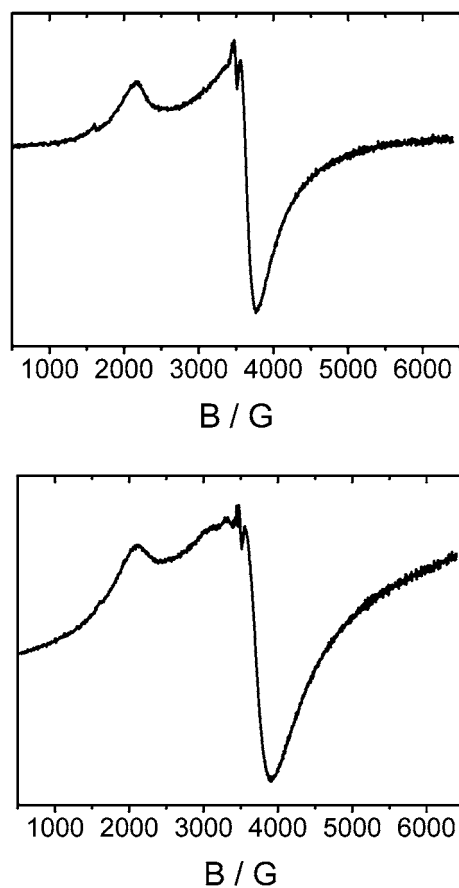
Figure 5. EPR spectrum of solid **2** (top) and **1** (bottom) at 110 K.

and in frozen solution. The g values are $g_{\parallel}$ = 3.203 and $g_{\perp}$ = 1.908 with g_{av} = 2.340 and Δg = 1.295. These data point to a substantial Pd^{III} character and, in addition, show that the unpaired electron in this low-spin d^7 metal ion does not reside in the d$_z^2$ orbital in the present case but instead in the d$_{yz}$ orbital partly elucidating why no Pd—Pd bond is observed in the described Pd^{III} complexes.[18]

If oxidation were to take place at the Fe center, a situation similar to 1,2,3,4,5-pentaphenylferrocenium or ferrocenium would have been expected. The absolute g values for **2** are much less extreme than for ferrocenium and accordingly the g-anisotropy (Δg) is smaller. These data together with the fact that the EPR signal for **2** was detected at 110 K uncover the substantial spin density at the Pd center and show the importance of a Fe^{II}/Pd^{III} resonance form for the present case. Absolute comparison with literature reported EPR spectra of Pd^{III} species is difficult, because most of the reported organometallic Pd^{III} complexes are dimeric containing a Pd—Pd bond thus making them EPR silent. Most of the few reported monomeric Pd^{III} species carry potentially redox-active ligands. In these cases substantial electron density resides on the organic part of the complexes thus drastically reducing the g-anisotropy and making the absolute g values closer to the free electron value.[4b−d] The present case has a substituted ferrocene part attached to the Pd center and this leads to a relatively high g-anisotropy. The value, however, is significantly smaller compared to that observed for ferrocenium hence supporting our formulation of a predominantly Fe^{II}/Pd^{III} form in the present case. The EPR spectrum of **1** is very similar to **2** (Figure 5, bottom).[19] The g values are $g_{\parallel}$ = 3.200 and $g_{\perp}$ =

1.915 with g_{av} = 2.420 and Δg = 1.285. In contrast, the one-electron oxidized form of the ligands is EPR silent down to 100 K.

2 was found to react with 3,5-di-*tert*-butyl catecholate (DTBC, Scheme 4) under an inert atmosphere producing an

Scheme 4. Formation of a Pd^{II} Bound Semiquinone Radical 5 from Pd^{III} Complex 2 with 3,5-Di-*tert*-butyl Catecholate
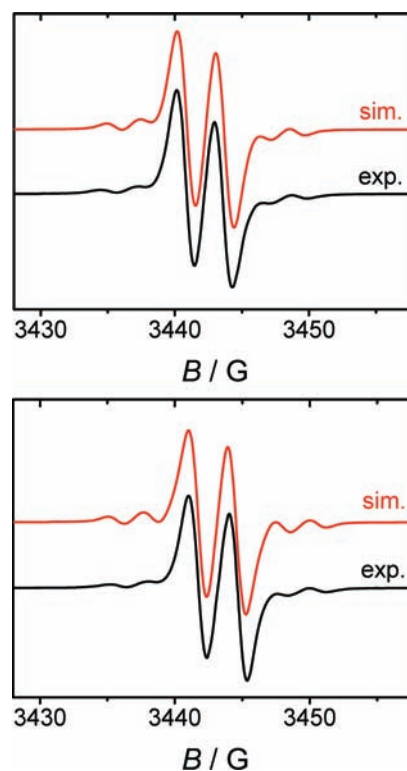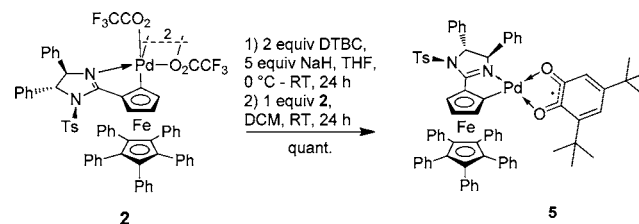

Figure 6. EPR spectrum of **2** + 3,5-*di-tert*-butyl catecholate (top) and **1** + 3,5-*di-tert*-butyl catecholate (bottom) recorded in CH$_2$Cl$_2$ at 295 K.

EPR signal (Figure 6) typical for a Pd^{II} bound semiquinone radical **5** which could be simulated with g = 2.0049, $A(^1H, I = 1/2)$ = 2.8 G, and $A(^{105}Pd, I = 5/2$, natural abundance =22.33%) = 2.1 G (Figure 6, top).[20]

Binding of 3,5-di-*tert*-butyl catecholate to **2** thus results in a reduction of Pd^{III} to Pd^{II} and a concomitant oxidation of the catecholate form to the semiquinone form **5** (or its geometric isomer which is not shown). Blind EPR runs in the absence of **2** did not produce such a spectrum. The presence of the ^{105}Pd satellites in the EPR spectrum and ESI mass spectra confirm the binding of **2** to the semiquinone radical ligand. Similar results were also obtained for **1** (Figure 6, bottom). The spectrum in this case could be simulated with g = 2.0048, $A(^1H,$

$I = 1/2) = 2.8$ G, and $A(^{105}\text{Pd}, I = 5/2,$ natural abundance $= 22.33\%) = 2.4$ G. With **2**, it was also possible to isolate the semiquinone bound metal complex which shows an identical EPR spectrum to the one generated in situ.

(Spectro)Electrochemical Studies. Cyclic voltammetry of **PPFIP-Cl** shows two one-electron oxidation processes at 0.11 and 0.23 V vs Fc/Fc$^+$ (Figure 7, top). These are attributed to
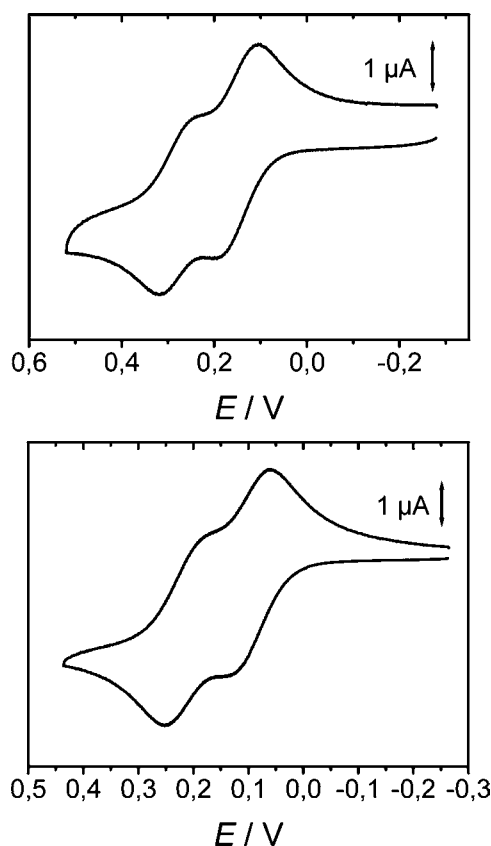

Figure 7. Cyclic voltammogram of **PPFIP-Cl** (top) and **PPFOP-Cl** (bottom) in CH$_2$Cl$_2$/0.1 M Bu$_4$NPF$_6$. Scan Rate: 100 mV s^{-1}. A gold electrode was used as the working electrode and Fc/Fc$^+$ was used as the internal standard.

the successive oxidation of the two Pd^{II} centers in a dimeric species, which also stays in a dinuclear state in solution after the first oxidation. **PPFOP-Cl** shows almost identical redox responses as **PPFIP-Cl** (Figure 7, bottom). The corresponding ligands show only one redox wave at 0.31 and 0.42 V, respectively (see the Supporting Information).

In order to shed more light into the redox processes UV−vis-NIR spectroelectrochemical measurements were carried out on **PPFIP-Cl** using an optically transparent thin layer electrochemical (OTTLE) cell. The native state of **PPFIP-Cl** shows a band at 515 nm that is assigned to a metal to ligand charge transfer (MLCT) transition. One-electron oxidation of this complex results in a high-energy shift of this band to 442 nm (Figure 8).

Additionally, a new broad band appears with a maximum at 915 nm. It is tempting to assign this band to an inter valent charge transfer (IVCT) transition as would be expected for a Pd^{II}/Pd^{III} mixed-valent situation. However, on further one-electron oxidation to the [**PPFIP-Cl**]$^{2+}$ form this band grows in intensity instead of disappearing. The same happens with the other bands seen in the UV−vis−NIR spectrum. Hence we
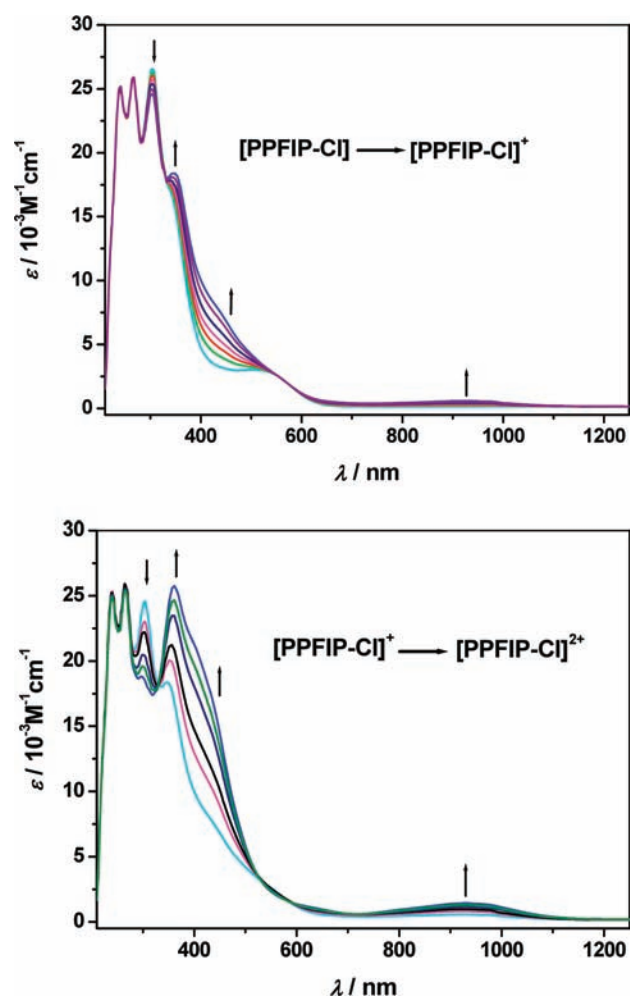

Figure 8. Changes in the UV−vis-NIR spectra of **PPFIP-Cl** during first (top) and second (bottom) oxidation in CH$_2$Cl$_2$/0.1 M Bu$_4$NPF$_6$ using OTTLE spectrolelectrochemistry.

tentatively assign the band at 915 nm to a d-d transition within the Pd^{III} level. The fact that it increases in intensity on successive oxidation processes supports our assignment. The small potential difference between the two redox waves in cyclic voltammetry already points to a negligible communication between the two metal centers in the mixed-valent form. This is also confirmed by the absence of an IVCT band which can be attributed to very weak electronic coupling between the metal centers in the mixed-valent state. Detailed assignments of the bands in the UV−vis−NIR spectra of the various redox forms will have to await high level theoretical calculations. Chemical oxidation of **PPFIP-Cl** with thianthrenium tetrafluoroborate delivered results that are identical to those observed with OTTLE spectroelectrochemistry (see Supporting Information). Thus redox titration of **PPFIP-Cl** with one equivalent of thianthrenium tetrafluoroborate delivered a spectrum that is identical to that obtained after the first redox wave with OTTLE spectroelectrochemistry. The same holds true for the second equivalent of thianthrenium tetrafluoroborate as well. These results in turn prove the one-electron nature of the redox waves. The complete reversibility of the redox processes as seen from 100% recovery of the starting material on reversing the scan in OTTLE spectroelectrochemistry together with the observance of perfect isosbestic points in the UV−vis−NIR spectra proves that the substances do not decompose in

solution. Additionally, we have used the Baranski method to determine the number of electrons in each redox wave.[21] These chronoamperometric measurements have given us clear proof of the one-electron nature of each of the redox waves.

The two-electron oxidized form of **PPFIP-Cl** and **PPFIP-OAc**, respectively, was also generated chemically by using an excess of thianthreniumtetrafluoroborate (**6**) in CH_2Cl_2 (Scheme 5).[22] Species **7a–c** generated by this method show EPR signals very similar to that of **1** (Figure 9).

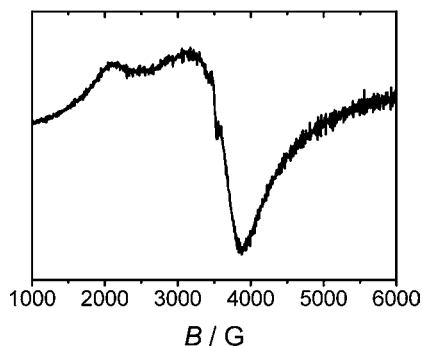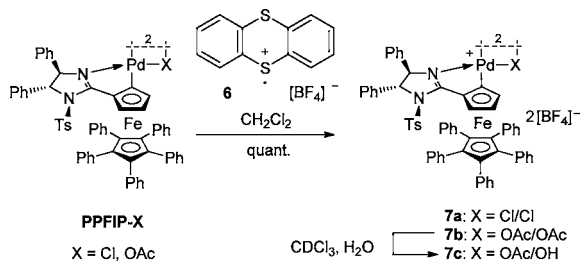**Scheme 5. Precatalyst Oxidation by Thianthrenium Tetrafluoroborate (6)**

PPFIP-X

X = Cl, OAc

$CDCl_3$, H_2O

7a: X = Cl/Cl
7b: X = OAc/OAc
7c: X = OAc/OH

Figure 9. EPR spectrum of **7c** in the solid state at 110 K. $g_\parallel = 3.303$ and $g_\perp = 1.927$ with $g_{av} = 2.472$ and $\Delta g = 1.376$.

Mössbauer Studies. Mössbauer experiments were carried out with the precatalyst **PPFIP-Cl** and the activated catalyst **2** at 40 K. The spectrum of **PPFIP-Cl** (Figure 10, A) consists of a doublet with an isomer shift δ_{IS} of 0.559(3) mm s^{-1} (relative to α-Fe) and a quadrupole splitting ΔE_Q of 2.389(5) mm s^{-1}. These values, especially the large quadrupole splitting ΔE_Q, are consistent with the formulation of the Fe site as ferrocene moiety.[23] The spectrum of **2** at 40 K (Figure 10, B) renders a doublet at an isomer shift δ_{IS} of 0.562(3) mm s^{-1} with a quadrupole splitting ΔE_Q of 2.351(6) mm s^{-1}. This very little change of the Mössbauer parameters indicates that the oxidation state of the Fe ion remains the same during oxidation of **PPFIP-Cl** to **2**. The slight decrease of the quadrupole splitting can be explained by the increasing charge withdrawal from the cyclopentadienyl ring due to the oxidation of the Pd ion.[24] In order to examine whether any valence tautomerism from a Fe^{II}Pd^{III} to a Fe^{III}Pd^{II} state might occur upon raising the temperature, the corresponding Mössbauer spectra of the samples were also recorded at room temperature. These spectra reveal doublets at isomer shifts δ_{IS} of 0.507(5) and 0.488(5) mm s^{-1} with quadrupole splittings ΔE_Q of 2.338(9) and 2.320(10) mm s^{-1} for **PPFIP-Cl** and **2**, respectively, thus providing no evidence for a change of oxidation states with increasing temperature. A similar reduction in size of the Mössbauer parameters with increasing temperatures is ususally
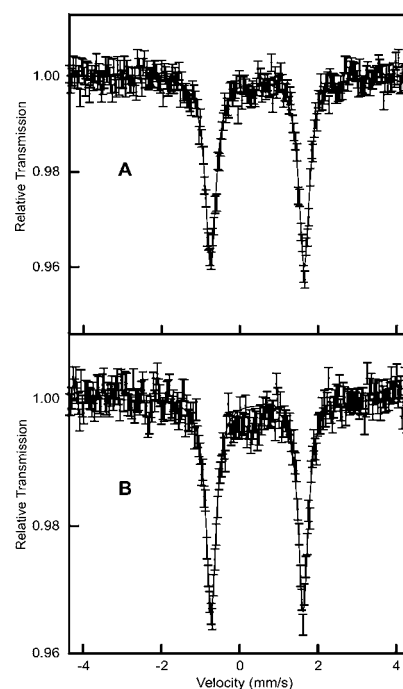
Figure 10. Mössbauer spectra of **PPFIP-Cl** (A) and **2** (B) recorded at 40 K. (Note: The isomer shifts in this Figure are given relative to the cobalt source, while the isomer shifts in the text are referenced versus an α-iron foil.)

observed also for other ferrocene molecules.[23] Overall, the Mössbauer spectroscopic results agree very well with those of XANES and EPR spectroscopy described above.

X-ray Crystal Structure Analysis. While all attempts to generate crystals of **1** and **2** suitable for X-ray crystal structure analysis have failed, **7c**, formed from **7b** by partial acetate/hydroxide ligand exchange (Scheme 5), provided appropriate crystals from wet $CDCl_3$.[25] Since BF_4^- is a poorly coordinating counterion, the Pd^{III} coordination sphere is square planar (Figure 11). The distance of two Cp rings (3.46 Å) of one ferrocene fragment is increased by ca. 0.13 Å as compared to structures previously obtained for **PPFOP-OAc** or **PPFIP-**
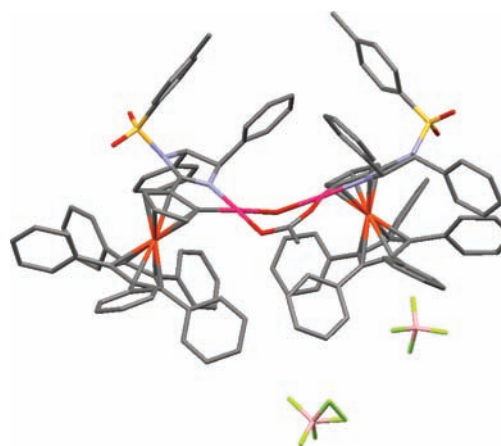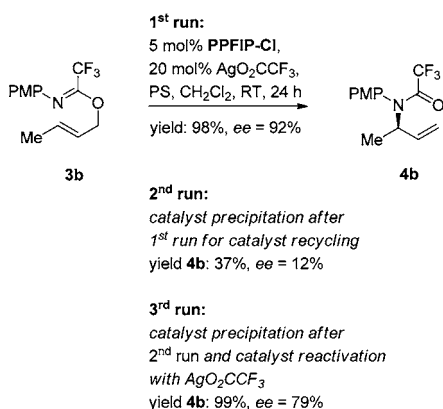
Figure 11. X-ray crystal structure of **7c** [color code: C (gray); B (gray-brown); F (green); N (blue); O (red); S (yellow); Fe (orange); Pd (pink)]. H atoms and one included water molecule per unit cell are omitted for clarity. One BF_4^- counterion shows a disorder in the solid state.

acac.[8d] This might be attributed to the lower electron density of the Cp owing to the more electron withdrawing Pd[III].[26] In **7c** the Fe−C distance of both C atoms directly connected to the Pd-centers is elongated by 0.051 − 0.095 Å as compared to **PPFIP-acac**.

2.3. Mechanistic Studies and Considerations. Recycling of the catalyst after aza-Claisen rearrangement has been reported to be inefficient as a result of catalyst deactivation.[8d] In the present study we found that after complete conversion of substrate **3b** (Scheme 6, after the first run) neither the solution

Scheme 6. Study of the Catalyst Deactivation and Reactivation (PS = Proton Sponge = 1,8-Bis(dimethylamino)naphthalene)

1st run:
5 mol% **PPFIP-Cl**,
20 mol% AgO₂CCF₃,
PS, CH₂Cl₂, RT, 24 h

yield: 98%, *ee* = 92%

2nd run:
catalyst precipitation after
1st run for catalyst recycling
yield **4b**: 37%, *ee* = 12%

3rd run:
catalyst precipitation after
2nd run and catalyst reactivation
with AgO₂CCF₃
yield **4b**: 99%, *ee* = 79%

of the reaction mixture nor precipitated catalyst (after addition of *n*-pentane) gave an EPR signal anymore, even with an exceptionally high precatalyst loading of 5 mol %, pointing to the formation of a diamagnetic complex. Fe K-edge XANES spectra of both the reaction solution and the precipitated catalyst revealed the presence of an Fe[II] species after catalysis, whereas Pd K-edge XANES spectra confirm that the diamagnetic species contains a Pd[II] center (see the Supporting Information).

^{1}H NMR spectra of the precipitated catalyst after the first run show somewhat broadened signals for the Cp and the benzylic imidazoline protons pointing to a diamagnetic major species which contains paramagnetic impurities. This recycled catalyst catalyzes the rearrangement with only moderate yield in a second run (Scheme 6), forming almost racemic product. Filtration of a solution of the precipitated catalyst over silica gel largely removed paramagnetic impurities and polar Pd salts resulting in a material with sharp ^{1}H NMR signals which was almost inactive in a subsequent run. However, reoxidation of precipitated catalyst after the second run with AgO₂CCF₃, followed by removal of excess silver salt by filtration, led again to high catalytic activity in a third run (Scheme 6). In addition, the product was formed again with a significant enantiomeric excess of 79%.[27]

These data support that the catalytically active Pd[III] species is deactivated during the catalysis process as a result of catalyst reduction by formation of a Pd[II]/Fe[II] species.[28] While the Pd[II]/Fe[II] system shows low activity, it can be reactivated by oxidation with Ag[I] regenerating the paramagnetic enantioselective catalyst. ESI-MS data of the reactivated catalyst for the third catalysis run have identified a monomeric oxidized complex carrying two trifluoroacetate counterions plus a neutral amide ligand derived from the rearrangement product of the previous

run.[29] This arguably suggests that not only the complex carrying neutral product, but also the active catalyst species with the coordinated neutral imidate substrate should be monomeric bearing two trifluoroacetate (**PPFIP**) or two nitrate ligands (**PPFOP**). Due to their paramagnetic character these species are not observable by ^{1}H NMR. However, ESI-MS data collected directly after the start of the catalytic process using substrate **3c** (for **3c** see Figure 12) confirm the presence of such a monomeric substrate-catalyst complex.
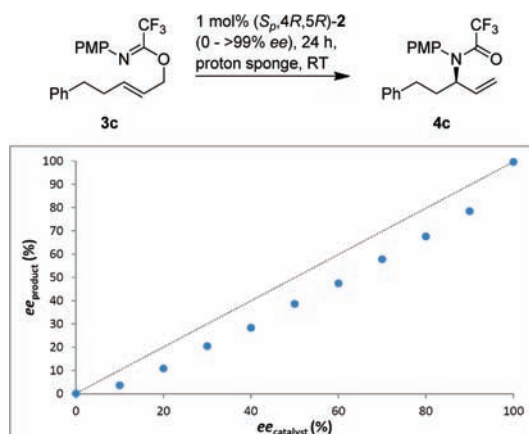

Figure 12. Negative nonlinear effect for the allylic imidate rearrangement of **3c** using (*Sp*,4*R*,5*R*)-**2** with catalyst *ee* values ranging from 0 - >99%. With almost enantiopure catalyst product **4c** is formed with 99.6% *ee*. The NLE suggests the existence of higher catalyst aggregates, most likely dimers, in equilibrium with the monomeric complex binding the substrate.

These monomeric complexes generated by either product or substrate coordination are most likely in equilibrium with a dimeric species such as compound **2**. This is supported by a (negative) nonlinear effect (NLE)[30] found for the rearrangement of substrate **3c** (Figure 12).

In a monomeric substrate complex, the 5-coordinated Pd center could either adopt a square pyramidal or a trigonal bipyramidal coordination sphere.[31] The former option is often preferred for 5-coordinate complexes of Pd.[31b] In addition, a trigonal bipyramidal geometry appears to be less likely in our case for steric reasons, because one ligand would have to point in the direction of the sterically demanding pentaphenyl-Cp spectator ligand. For the same reason, an octahedral complexation geometry, which is in general favored for Pd[III] complexes, is unlikely for pentaphenylferrocene palladacycles with Pd[III].

Prior to the studies described herein, our initially reported working hypothesis for the rearrangement of allylic trifluoroacetimidates with square planar Pd[II] catalysts could rationalize the observed high enantioselectivities,[8d] the efficient kinetic resolution of chiral racemic substrates[8e] and the stereospecificity using different geometric isomers.[8d] *E*- and *Z*-olefins in general provide the generated stereocenter in the product with the opposite configuration.[8d] As a consequence, also quaternary stereocenters can be formed with excellent stereocontrol starting from geometrically pure trisubstituted olefins.[8d] Even a trisubstituted olefin, in which the *E*- and *Z*-double bond substituents have an identical size, like CH₃ and CD₃, provided an almost enantiopure product.[8b]

This observed stereospecificity for the C−N bond formation suggests that the enantioselectivity (pre)determining step should be the face selective coordination of the olefin moiety

to the Pd center. Our modified working hypothesis for a Pd[III] center differs from the initial model only by an additional counterion in the apical position (Figure 13),[31b] and is thus still able to rationalize the stereospecificity and the high enantioselectivity.
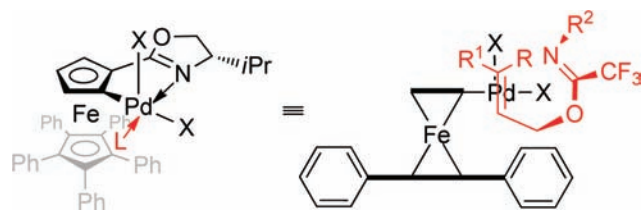

Figure 13. Working hypothesis to rationalize the stereospecific reaction outcome for the rearrangement of allylic trifluoroacetimidates. Face-selective olefin coordination followed by outer-sphere attack of the imidate N-atom at the olefin can explain why the configuration of the new stereocenter switches for different geometric isomers and why quaternary stereocenters can be generated with high stereocontrol.

Based on the observed *trans*-effect for square planar palladacycles with a Pd[II] center,[8d,g] we speculate that the neutral olefin ligand coordinates *trans* to the imidazoline N atom. This coordination triggers an attack of the nucleophilic imidate N atom at the olefin from the face remote to the Pd center (Figure 13).[28] In an orientation of the olefin part parallel to the ferrocene axis, i.e., perpendicular to the Pd square plane, which would be favored for square planar and octahedral complexes,[31a] the sterically less demanding C-1 methylene moiety should point toward the bulky Ph_5C_5 spectator ligand to minimize repulsive steric interactions. Sterically less demanding counterions X^- like nitrate or trifluoroacetate in apical position would support this preference. In the suggested reactive coordination mode the relatively bulky imidate moiety would avoid the ferrocene core, while coordination of the enantiotopic olefin face would result in steric repulsion.

3. SUMMARY

In conclusion, a combination of spectroscopic and electrochemical methods demonstrates that the most efficient catalysts for the asymmetric rearrangement of allylic trifluoroacetimidates unexpectedly possess in the activated form a Pd[III] center bound to an unchanged ferrocene core (Fe[II]). These are the first recognized Pd[III] complexes acting as enantioselective catalysts. Moreover, these complexes are the first recognized dimeric paramagnetic organometallic Pd[III]/Pd[III] complexes.

4. EXPERIMENTAL SECTION

X-ray Absorption. X-ray absorption measurement at the Pd K-edge (24.350 keV) were carried out at beamline X1 of Hasylab (Hamburg, Germany) under ambient conditions at 20 °C. A Si(311) double crystal monochromator was used. The second monochromator crystal was tilt for optimal harmonic rejection. The energy resolution for the Pd K-edge energy is estimated to 1.0 eV. The spectra were recorded in transmission mode with ionization chambers. Energy calibration was performed with a palladium metal foil. To avoid errors in the XANES region due to small changes in the energy calibration between two measurements, all spectra were corrected to the theoretical edge energy of Pd foil, which was measured every scan. Two spectra of each sample were averaged in order to reduce the spectral noise as well as to check for changes in course of the measurements. The solid samples were mixed with degassed cellulose and pressed into pellets before sealing them. Sample handling was carried out in a glovebox.

Data evaluation of the K-edge EXAFS spectra started with background absorption removal from the experimental absorption spectrum by subtracting a Victoreen-type polynomial with the WINXAS program package.[32] The background-subtracted spectrum was then convoluted with a series of increasingly broader Gauss functions and the common intersection point was taken as energy E_0.[33] To determine the smooth part of the spectrum, corrected for pre-edge absorption, a piecewise polynomial was used. It was adjusted in such a way that the low-R components of the resulting Fourier transform were minimal. After division of the background−subtracted spectrum by its smooth part, the photon energy was converted to photoelectron wave numbers k. The resulting $\chi(k)$ function was weighted with k^3. Data analysis was performed in k-space according to the curved wave formalism.[34] EXCURV98 with XALPHA phase and amplitude functions was used to fit the data.

Measurement at the Pd L_3-edge (3.173 keV) were performed at the XAS-beamline of ANKA (Karlsruhe, Germany). In case of these low-energy measurements, the sample powders were placed between 14 μm Kapton foils using a 50 μm spacer and sealed before removing it from the inert atmosphere. Spectra were collected in transmission mode using ionization chambers. A 1 cm path length was used which was purged with helium. Air was not completely removed from the beam path. The remaining argon K-edge signal (3.202 keV) from air was used for energy calibration on the price of a very short available normalization range. Normalization was carried out in the same way for all the samples, using identical pre-edge ranges.

EDX Measurements. EDX measurements were carried out on a Jeol −6490LA instrument with an acceleration voltage of 15 kV.

EPR Spectroscopy. EPR spectra in the X band were recorded with a Bruker System EMX connected with an ER 4131 VT variable temperature accessory. EPR simulations were carried out using the EasySpin software.[35]

Cyclic Voltammetry. Cyclic voltammetry was carried out in 0.1 M Bu_4NPF_6 solution using a three-electrode configuration (gold working electrode, Pt counter electrode, Ag wire as pseudoreference) and a PAR 273 potentiostat and function generator. The ferrocene/ferrocenium (Fc/Fc$^+$) couple served as internal reference.

UV−Vis−NIR Spectroelectrochemistry. UV−vis−NIR spectroelectrochemistry was carried out using an optically transparent thin layer electrochemical (OTTLE) cell and a J & M TIDAS spectrometer.[36]

Mössbauer. Mössbauer spectra were recorded using a conventional spectrometer (Wissel GmbH) in the constant acceleration mode. The temperature can be maintained between 6K and 400K by a closed-cycle cryostat unit of Advanced Research Systems Inc.. The sample holder is mounted on the tip of the second stage heat station of the expander unit DE204SF inside a radiation shield and a vacuum shroud. The expander unit is decoupled from the vibrations of the compressor ARS-4HW by a DMX20−41 interface. The temperature is controlled by a Lakeshore 331S unit. Approximately 50 mg of sample in a Teflon container are placed in the sample holder. The windows of the vacuum shroud are made of berrylium. The spectra were analyzed by least-squares fits using a Lorentzian line shape with the program WinNormus-for-Igor Version 2.0. The isomer shifts are given relative to an α-iron foil at room temperature.

■ ASSOCIATED CONTENT

Ⓢ Supporting Information

General experimental, synthetic, and spectral information. This material is available free of charge via the Internet at http://pubs.acs.org.

■ AUTHOR INFORMATION

Corresponding Author

bauer@chemie.uni-kl.de; sarkar@iac.uni-stuttgart.de; krueger@chemie.uni-kl.de; rene.peters@oc.uni-stuttgart.de

■ REFERENCES

(1) (a) Powers, D. C.; Ritter, T. *Nat. Chem.* **2009**, *1*, 302. (b) Deprez, N. R.; Sanford, M. S. *J. Am. Chem. Soc.* **2009**, *131*, 11234. (c) Powers, D. C.; Geibel, M. A. L.; Klein, J. E. M. N.; Ritter, T. *J. Am. Chem. Soc.* **2009**, *131*, 17050. (d) Powers, D. C.; Benitez, D.; Tkatchouk, E.; Goddard, W. A. III; Ritter, T. *J. Am. Chem. Soc.* **2010**, *132*, 14092. (e) Powers, D. C.; Xiao, D. Y.; Geibel, M. A. L.; Ritter, T. *J. Am. Chem. Soc.* **2010**, *132*, 14530.

(2) (a) Cotton, F. A.; Gu, J.; Murillo, C. A.; Timmons, D. J. *J. Am. Chem. Soc.* **1998**, *120*, 13280. (b) Cotton, F. A.; Koshevoy, I. O.; Lahuerta, P.; Murillo, C. A.; Sanaú, M.; Ubeda, M. A.; Zhao, Q. *J. Am. Chem. Soc.* **2006**, *128*, 13674. (c) Penno, D.; Lillo, V.; Koshevoy, I. O.; Sanaú, M.; Ubeda, M. A.; Lahuerta, P.; Fernández, E. *Chem.—Eur. J.* **2008**, *14*, 10648. (d) Pd₂⁵⁺ species: Berry, J. F.; Bill, E.; Bothe, E.; Cotton, F. A.; Dalal, N. S.; Ibragimov, S. A.; Kaur, N.; Liu, C. Y.; Murillo, C. A.; Nellutla, S.; North, J. M.; Villagrán, D. *J. Am. Chem. Soc.* **2007**, *129*, 1393.

(3) (a) Khusnutdinova, J. R.; Rath, N. P.; Mirica, L. M. *J. Am. Chem. Soc.* **2010**, *132*, 7303. (b) Khusnutdinova, J. R.; Rath, N. P.; Mirica, L. M. *J. Am. Chem. Soc.* **2012**, *134*, 2414.

(4) Other characterized Pd^III complexes are also rare: (a) Tressaud, A.; Khairoun, S.; Dance, J. M.; Hagenmuller, P. *Z. Anorg. Allg. Chem.* **1984**, *517*, 43. (b) Blake, A. J.; Holder, A. J.; Hyde, T. I.; Schröder, M. *J. Chem. Soc., Chem. Commun.* **1987**, 987. (c) Blake, A. J.; Gordon, L. M.; Holder, A. J.; Hyde, T. I.; Reid, G.; Schröder, M. *J. Chem. Soc., Chem. Commun.* **1988**, 1452. (d) Blake, A. J.; Reid, G.; Schröder, M. *J. Chem. Soc., Dalton Trans.* **1990**, 3363. (e) McAuley, A.; Whitcombe, T. W. *Inorg. Chem.* **1988**, *27*, 3090. (f) Jasper, S. A. Jr.; Huffman, J. C.; Todd, L. J. *Inorg. Chem.* **1998**, *37*, 6060.

(5) (a) Lanci, M. P.; Remy, M. S.; Kaminsky, W.; Mayer, J. M.; Sanford, M. S. *J. Am. Chem. Soc.* **2009**, *131*, 15618. (b) Cationic adducts of Pt^II and Ag^I have previously been reported: Moret, M.-E.; Chen, P *J. Am. Chem. Soc.* **2009**, *131*, 5675. (c) Arsenault, G. L.; Anderson, C. M.; Puddephatt, R. J. *Organometallics* **1988**, *7*, 2094.

(6) Monomeric organometallic Pd^III intermediates have been proposed: (a) Boisvert, L.; Denney, M. C.; Kloek Hanson, S.;

Goldberg, K. I. *J. Am. Chem. Soc.* **2009**, *131*, 15802. (b) Manolikakes, G.; Knochel, P. *Angew. Chem., Int. Ed.* **2009**, *48*, 205.

(7) Inorganic complexes: Khusnutdinova, J. R.; Rath, N. P.; Mirica, L. M. *Angew. Chem., Int. Ed.* **2011**, *50*, 5532.

(8) (a) Weiss, M. E.; Fischer, D. F.; Xin, Z.-q.; Jautze, S.; Schweizer, W. B.; Peters, R. *Angew. Chem., Int. Ed.* **2006**, *45*, 5694. (b) Fischer, D. F.; Xin, Z.-q.; Peters, R. *Angew. Chem., Int. Ed.* **2007**, *46*, 7704. (c) Xin, Z.-q.; Fischer, D. F.; Peters, R. *Synlett* **2008**, 1495. (d) Fischer, D. F.; Barakat, A.; Xin, Z.-q.; Weiss, M. E.; Peters, R. *Chem.—Eur. J.* **2009**, *15*, 8722. (e) Peters, R.; Xin, Z.-q.; Maier, F. *Chem. Asian J.* **2010**, *5*, 1770. Related catalysts: (f) Peters, R.; Xin, Z.-q.; Fischer, D. F.; Schweizer, W. B. *Organometallics* **2006**, *25*, 2917. (g) Jautze, S.; Seiler, P.; Peters, R. *Chem.—Eur. J.* **2008**, *14*, 1430. (h) Jautze, S.; Seiler, P.; Peters, R. *Angew. Chem., Int. Ed.* **2007**, *46*, 1260.

(9) Reviews: (a) Nomura, H.; Richards, C. J. *Chem. Asian J.* **2010**, *5*, 1726. (b) Peters, R.; Fischer, D. F.; Jautze, S. *Top. Organomet. Chem.* **2011**, *33*, 139. (c) Jautze, S.; Peters, R. In *Science of Synthesis: Stereoselective Synthesis*; Evans, P. A., Ed.; Thieme: Stuttgart, 2011; Vol. 3, Chapter 3.10, pp 443−467.

(10) (a) Anderson, C. E.; Donde, Y.; Douglas, C. J.; Overman, L. E. *J. Org. Chem.* **2005**, *70*, 648. (b) Remarchuk, T. P. Ph.D. Dissertation, University of California (Overman group): Irvine, CA, 2003; pp 175-235. (c) For a Co sandwich complex as catalyst, see: Overman, L. E.; Owen, C. E.; Pavan, M. M. *Org. Lett.* **2003**, *5*, 1809.

(11) Balasubramanian, M.; Giacomini, M. T.; Lee, H. S.; McBreen, J.; Sukamto, J. H. *J. Electrochem. Soc.* **2002**, *149*, D137.

(12) (a) Bauer, M.; Kauf, T.; Christoffers, J.; Bertagnolli, H. *Phys. Chem. Chem. Phys.* **2005**, *7*, 2664. (b) Farges, F.; Rossano, S.; Lefrére, Y.; Wilke, M.; Brown, G. E. Jr. *Phys. Scripta T* **2005**, *115*, 957.

(13) Westre, T. E.; DiCicco, A.; Filliponi, A.; Natoli, C.; Hedman, B.; Solomon, E. I.; Hodgson, K. O. *J. Am. Chem. Soc.* **1995**, *117*, 1566.

(14) Boysen, R. B.; Szilagyi, R. K. *Inorg. Chim. Acta* **2008**, *361*, 1047.

(15) Bauer, M.; Müller, S.; Kickelbick, G.; Bertagnolli, H. *New J. Chem.* **2007**, *31*, 1950.

(16) Guilera, G.; Newton, M. A.; Polli, C.; Pascarelli, S.; Guino, M.; Hii, K. H. *Chem. Commun.* **2006**, 4306.

(17) (a) Prins, R.; Reinders, F. J. *J. Am. Chem. Soc.* **1969**, *91*, 4929. (b) Fritz, H. P.; Keller, H. J.; Schwarzhans, K. E. *J. Organomet. Chem.* **1966**, *6*, 652.

(18) Mabbs, F. E.; Collison, D. *Electron Paramagnetic Resonance of d Transition Metal Compounds*; Elsevier Science Publishers: Amsterdam, The Netherlands, 1992.

(19) In contrast, activated ferrocene oxazoline palladacycles with 5 H-atoms at Cp' are better described as ferrocenium species (see ref 10b). This might in part be explained by the different redox potentials of pentaphenylferrocene [+743 mV in acetonitrile (Ag/AgCl)] and ferrocene [433−493 mV]: Schumann, H.; Lentz, A.; Weimann, R.; Pickardt, J. *Angew. Chem., Int. Ed.* **1994**, *33*, 1731 and cited references..

(20) Weil, J. A.; Bolton, J. R. *Electron Paramagnetic Resonance*, 2nd ed.; John Wiley & Sons, Inc.: Hoboken, NJ.

(21) Baranski, A. S.; Fawcett, W. R.; Gilbert, C. M. *Anal. Chem.* **1985**, *57*, 166.

(22) Connelly, N. G.; Geiger, W. E. *Chem. Rev.* **1996**, *96*, 877.

(23) Fluck, E.; Hausser, F. *Z. Anorg. Allg. Chem.* **1973**, *396*, 257.

(24) Neshvad, G.; Roberts, R. M. G.; Silver, J. *J. Organomet. Chem.* **1982**, *236*, 349.

(25) Supplementary crystallographic data for **7c** have been deposited with the Cambridge Crystallographic Data Centre as deposition 831695. This material is available free of charge via the Internet at http://pubs.acs.org and http://www.ccdc.cam.ac.uk/products/csd/request/.

(26) In ferrocenium salts [C₁₀H₁₀Fe]X the Cp distances to Fe are usually also slightly larger as compared to ferrocene with Fe-C distances, which are in average elongated by ca. 0.024 Å: (a) Martinez, R.; Tirpicchio, A. *Acta Crystallogr.* **1990**, *C46*, 202. (b) Churchill, M. R.; Landers, A. G.; Rheingold, A. L. *Inorg. Chem.* **1981**, *20*, 849 However, we can rule out a species with ferrocenium character by the XANES and Mössbauer studies (see above).

4692

dx.doi.org/10.1021/ja2098222 | *J. Am. Chem. Soc.* 2012, 134, 4683−4693

(27) For other applications of ferrocene imidazoline metallacycles in asymmetric catalysis see: (a) Weber, M.; Jautze, S.; Frey, W.; Peters, R. *J. Am. Chem. Soc.* **2010**, *132*, 12222. (b) Huang, H.; Peters, R. *Angew. Chem., Int. Ed.* **2009**, *48*, 604. (c) Jautze, S.; Peters, R. *Angew. Chem., Int. Ed.* **2008**, *47*, 9284. Synthetic studies: (d) Peters, R.; Fischer, D. F. *Org. Lett.* **2005**, *7*, 4137. (e) Jautze, S.; Diethelm, S.; Frey, W.; Peters, R. *Organometallics* **2009**, *28*, 2001. (f) For recycling attempts using an immobilized catalyst, see: Nomura, H.; Richards, C. *J. Chem.—Eur. J.* **2007**, *13*, 10216.

(28) We can exclude a radical mechanisms for the allylic imidate rearrangement with high certainty, because the rearrangement works with almost equal efficiency in the presence of TEMPO (1 equiv) as radical scavenger or if the reaction is performed under air.

(29) ESI-MS *m/z*: 1513.18 ([ligand+Pd+$(O_2CCF_3)_2$+N-PMP-trifluoroacetamide+Na]$^+$, 20%), 1406.13 ([ligand+Pd+$(O_2CCF_3)_2$+trifluoroacetamide+Na]+, 3%), 1318.26 ([ligand+Pd+**4b**]$^+$, 2%), 1045.17 ([ligand+Pd]$^+$, 100%), 890.14 ([ligand+Pd − Ts]$^+$, 5%).

(30) Satyanarayana, T.; Abraham, S.; Kagan, H. B. *Angew. Chem., Int. Ed.* **2009**, *48*, 456.

(31) (a) Albright, T. A.; Hoffmann, R.; Thibeault, J. C.; Thorn, D. L. *J. Am. Chem. Soc.* **1979**, *101*, 3801. (b) Cross, R. J. *Adv. Inorg. Chem.* **1989**, *34*, 219.

(32) Ressler, T. *J. Synchrotron Rad.* **1998**, *5*, 118.

(33) Ertel, T. S.; Bertagnolli, H.; Hückmann, S.; Kolb, U.; Peter, D. *Appl. Spectrosc.* **1992**, *46*, 690.

(34) Binsted, N.; Hasnain, S. S. *J. Synchrotron Rad.* **1996**, *3*, 185.

(35) Stoll, S.; Schweiger, A. *J. Magn. Reson.* **2006**, *178*, 42.

(36) Krejcik, M.; Danek, M.; Hartl, F. *J. Electroanal. Chem. Interfacial Electrochem.* **1991**, *317*, 179.